Available online at www.sciencedirect.com

SciVerse ScienceDirect

Ceramics International 38 (2012) 1359–1363

CERAMICS INTERNATIONAL

www.elsevier.com/locate/ceramint

Effect of oxygen substitution by nitrogen on magnetic and transport properties in Sr_2FeMoO_6 compound

Guoyan Huo *, Jingjuan Wen, Chenghui Zhang, Minghui Ren

School of Chemistry and Environmental Science, Hebei University, Baoding 071002, PR China

Received 7 May 2011; received in revised form 4 September 2011; accepted 5 September 2011
Available online 10 September 2011

Abstract

The result of Fullprof_suite refinement shows that the structure of $Sr_2FeMo(O_{0.889}N_{0.111})_6$ is assigned to tetragonal system with space group *I*4/*m* and its cell parameters are $a = 0.559250(8)$ nm and $c = 0.789842(19)$ nm. The *M–T* curve demonstrates the magnetic transition temperature being over 300 K. Isothermal magnetization shows that the saturation and spontaneous magnetization are 1.29 and 0.87 μ_B/fu at 300 K, respectively. The sample shows a large magnoresistance in a 0.5 T magnetic field. The electrical transport behavior in the temperature range from 108 to 274 K is dominated by electron–phonon scattering under a zero magnetic field. However, under a magnetic field of 0.5 T the electron–electron and electron–magnon scattering control electrical transport behavior in the temperature range from 145 to 267 K and electrical transport property is governed by electron–phonon scattering in the temperature region of 97–130 K.

Keywords: Ceramic composites; Crystal structure; Magnetic materials; Electrical transport behavior

1. Introduction

The recent discovery of half-metallic transition metal oxides with ordered double perovskite (DP) structure $A_2B'B''O_6$ (A is an alkaline-earth element, B′ and B″ are transition metal elements) has stimulated research on the properties of them owing to their remarkable tunneling and intergrain magnetoresistance (*MR*) around room temperature [1–3]. Among the DP compounds synthesized so far, Sr_2FeMoO_6 is the most extensively studied, due to the overcome severe temperature limitation of the manganese perovskites and high Curie temperature $T_C \approx 415$ K. In the ideal Sr_2FeMoO_6 structure, the $Sr(FeMo)O_3$ perovskite building-blocks form a NaCl-superlattice in such a way that the Fe–Fe (Mo–Mo) distance is doubled with respect to elementary perovskite unit cell. In a simple picture, the ferrimagnetic structure can be described as an ordered array of parallel Fe^{3+} ($S = 5/2$) magnetic moments, antiferromagnetically coupled with Mo^{5+} ($S = 1/2$) spins [4]. The saturation magnetization derived from this ideal model, at low temperature, would be of 4 μ_B per formula unit (fu). In the real world, such a large magnetization value has not been obtained for bulk Sr_2FeMoO_6 up to date; instead smaller value below 3.7 μ_B/fu has been reported [1,5,6]. The origin of the difference between experimental and theoretical magnetization can be explained by the so-called antisite B-cation disorder, implying that some Mo^{5+} cations occupy the positions of Fe^{3+} cations, and vice versa. The actual degree of order depends on, on the one hand, the synthesis conditions; on the other hand, the charge and size differences between B-site cations [7].

In the recent years, many efforts have been dedicated to tune and optimize the *MR* properties of Sr_2FeMoO_6-related double perovskites, by doping at both Sr and (Fe,Mo) sublattices. Sr atoms have been incompletely substituted by La, Ca or Ba atoms, leading to different modifications of the physical properties [8–10]. To our knowledge, however, very few references to anion doping in DP Sr_2FeMoO_6 have been found. A study of nitrogen-doped on oxygen site in this compound may throw some light on its physical properties. In this paper, we study the crystalline structure, magnetic and transport properties of DP polycrystalline $Sr_2FeMo(O_{0.889}N_{0.111})_6$.

* Corresponding author. Tel.: +86 3125079359; fax: +86 3125079525.
E-mail addresses: huoertang@yahoo.com.cn, guoyanhuo@yahoo.com.cn (G. Huo).

0272-8842/$36.00
doi:10.1016/j.ceramint.2011.09.014

2. Experimental

The polycrystalline $Sr_2FeMo(O_{0.889}N_{0.111})_6$ sample has been synthesized by standard solid state reaction technique. The raw materials, Fe_2O_3 (preheated at 350 °C for 3 h), $SrCO_3$ (preheated at 800 °C for 5 h), and $(NH_4)_6Mo_7O_{24}{\cdot}4H_2O$ of high purity (more than 99.95%) were mixed by hand in an agate mortar for at least 45 min. Then it was pressed into pellets under 10 MPa pressure for 1 min, following preheating in air at 800 °C for 8 h. The calcined mixture was pulverized and pressed into pellets. The pellets were sintered at 900 °C for 8 h in a steam of 7% H_2/Ar. Following the sintered sample was ground and pressed into pellets. These pellets were heated at 1000 °C for 10 h in a steam of 7% H_2/Ar. The thermal ammonolysis of sample was performed at 1100 °C for 8 h in a steam of 5:1:14 NH_3/H_2/Ar. After the ammonolysis reaction the sample was ground and pressed into pellets. The pellets were sintered at 1100 °C for 16 h with intermediated grindings and finally cooled down to room temperature in furnace. Phase analysis and characterization were carried out by X-ray diffraction (XRD) using Cu Kα radiation on Rigaku model TTR-III X-ray diffractometer. The nitrogen amount was determined by spectroscopic analysis.

Temperature dependence of magnetization was measured by a vibrating-sample magnetometer in a 0.5 T magnetic field over the temperature range from 80 to 300 K. Transport properties were determined by a standard four-probe DC method in the temperature range from 78 to 300 K.

3. Results and discussion

The XRD data of powdered sample were collected at room temperature and the pattern is shown in Fig. 1. One can see from Fig. 1 that the XRD pattern shows DP compound $Sr_2FeMo(O_{0.889}N_{0.111})_6$ as dominant phase. Small amount of impurities were detected based on XRD pattern. The diffraction peaks of main phase $[Sr_2FeMo(O_{0.889}N_{0.111})_6]$ could be indexed in tetragonal system with space group *I*4/*m*. In order to illustrate the correction of the structure and to obtain more structural parameters the Rietveld refinement was carried out using space group *I*4/*m*. As some structural parameters of the refinement results are unreasonable, we adjusted the coordinates of O1 from (0 0 0.263) to (0 0 0.237(0.5–0.263)) and the coordinates of O2 (0.232 0.259 0) were remained. In the following refinement process the coordinates of O1 and O2 are fixed the values given above. Fig. 1 also shows the result of Fullprof_suite refinement with space group *I*4/*m*. The lattice parameters are obtained from the refinement results and are: $a = 0.559250(8)$ nm and $c = 0.789842(19)$ nm. The lattice parameters are slightly larger than those reported by Retuerto et al., Chan et al. and Wang et al., $a = 0.55686$ nm, $c = 0.79007$ nm; $a = 0.55686$ nm, $c = 0.78985$ nm and $a = 0.55766$ nm, $c = 0.789387$ nm [11–13]. This indicates that some oxygen atoms are replaced by nitrogen atoms. The refined structural and occupied parameters are detailed in Table 1. One can see from Table 1 that there is iron deficiency in the sample. Small amount of iron form iron oxide based on refinement results. Some selected interatomic distances and bond angles are given in Table 2. After refinement the reliability factors R_p and R_{wp} are 7.74 and 12.1, respectively. You can see from Table 2 that the $Fe(O,N)_6$ and $Mo(O,N)_6$ octahedra are elongated and flattened along *c*-axis, respectively and that the bond angles of Fe–$(O,N)_1$–Mo and Fe–$(O,N)_2$–Mo are 180.0° and 173.8°, respectively. The average bond lengths of Fe–(O,N) and Mo–(O,N) are 0.2046 and 0.1908 nm, respectively. The distance differences between B–(O,N)1 and B–(O,N)2 are 0.0061 and −0.0072 nm for B = Fe and Mo, respectively (see Table 2). We expect the reasons as following. On the one hand, the bonds of N–Fe and N–Mo show more covalent characteristic than those of O–Fe and O–Mo, respectively. In the covalent bonds, nitrogen and oxygen can form 3 and 2 covalent bands, respectively. Therefore, the bridge nitrogen connects iron or molybdenum with double covalent bond at one side and connects molybdenum or iron with single covalent bond at another site. The length of double covalent bond of Fe and N or Mo and N is shorter than that of single covalent bond between them. It is also shorter than length of single covalent band of Fe and O or Mo and O. However, the length of single covalent bond of Fe and N or Mo and N is longer than that of single covalent bond of Fe and O or Mo and O. On the other hand, the nitrogen takes −3 oxidation state and corresponding amount of molybdenum must be +6 oxidation state based on electrical neutral principle and the radius of Mo(VI) is smaller than that of Mo(V). This leads to the $Fe(O,N)_6$ and $Mo(O,N)_6$ octahedra are elongated and flattened along *c*-axis, respectively, and the cell

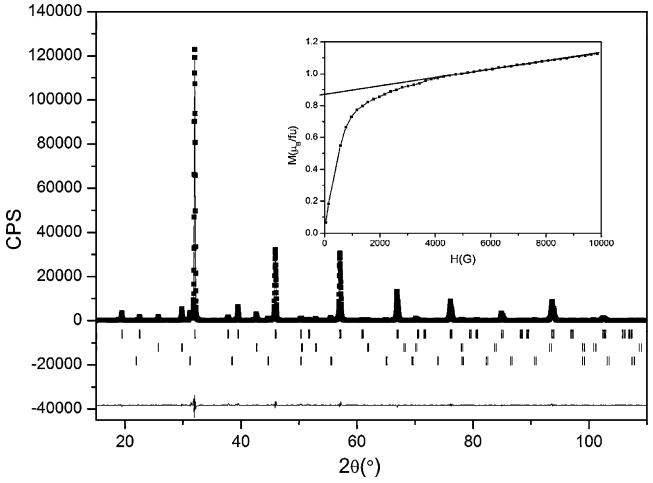

Fig. 1. X-ray diffraction pattern of $Sr_2FeMo(O,N)_6$ sample; inset: *M*–*H* curve at 300 K.

Table 1
Structural and occupied parameters obtained from refinement results.

	x	*y*	*z*	Occ.
Sr	0.000	0.500	0.250	0.972
Fe/Mo	0.000	0.000	0.000	0.750/0.250
Mo/Fe	0.000	0.000	0.500	0.902/0.098
(O,N)1	0.000	0.000	0.237(4)	1.000
(O,N)2	0.232(2)	0.259(1)	0.000	1.000

Table 2
Selected interatomic distances (nm) and bond angles obtained from refinement results.

Sr–(O,N)		Fe–(O,N)		Mo–(O,N)		Fe–(O,N)–Mo	
Sr–(O,N)1	0.2798(3) × 4	Fe–(O,N)1	0.2077(3) × 2	Mo–(O,N)1	0.1872(3) × 2	Fe–(O,N)1–Mo	180.0(5)
Sr–(O,N)2	0.2720(2) × 4	Fe–(O,N)2	0.2016(5) × 4	Mo–(O,N)2	0.1944(4) × 4	Fe–(O,N)2–Mo	173.8(2)
Sr–(O,N)2	0.2871(2) × 4						

parameters are slightly larger than those of Sr_2FeMoO_6 compound. Distance between Fe and Mo in *z*-axis (0.3949 nm) is smaller than that in *xy* plane (0.3960 nm), indicating that nitrogen prefers to replace oxygen in *ab* plane based on the analysis mentioned above. The calculated tolerance, *t*, of Sr_2FeMoO_6 is 0.9905. Substitution of oxygen by nitrogen causes *t* decrease to 0.9889 as the radius of oxygen (1.40 Å) is smaller than that of nitrogen (1.50 Å). The angle of Fe–$(O,N)_2$–Mo is 173.8° and the ratio of $c/\sqrt{2}a$ is 0.9987. In order to get some insight into the cation distributions, the bond-valence sum was calculated according to Brown model [14]. The calculated valence for Sr is +1.945. The Fe cation exhibits the valence +2.844. The calculated valence state of Mo is +5.818. These values in the oxidation states of Sr, Fe and Mo agree with those we expect. The increase in bond valence of Mo is correlated with N-doping as the oxidation state of nitrogen is −3.

The temperature dependence of magnetization, measured in a magnetic field of 0.5 T, is shown in Fig. 2. It is evident to see from *M–T* curve that no Curie temperature (T_C) appears in this temperature range, indicating that the T_C of $Sr_2FeMo(O_{0.889}N_{0.111})_6$ sample is higher than 300 K. It can also be seen from Fig. 2 that the magnetization changes slightly large from 1.22 μ_B at 80 K to 0.79 μ_B at around 300 K. It can conjecture that the ferromagnetic interaction is dominated in the magnetic regime from the *M–T* curve. We can see from Fig. 2 that a sharp decrease in magnetization appears at about 115 K on the curve, indicating that the magnetic structure appears a change induced by incorporation effect of magnetic field and temperature (see following). In order to understand the magnetic properties we fitted the thermal magnetization to Bloch's law $M = M_0(1 - AT^{3/2})$. The fitting of spontaneous magnetization to $T^{3/2}$ is shown in Fig. 3. It can be seen from Fig. 3 that fitting experimental data to Bloch' law is well in temperature range from 140 to 285 K, indicating that in this temperature range the spontaneous magnetization follows spin-wave model. In the low temperature range we fitted the spontaneous magnetization to Stoner's band model $M = M_0(1 - BT^2)$. The fitting of spontaneous magnetization to T^2 is shown in inset of Fig. 3. This indicates that the anomaly at about 115 K on the *M–T* curve is a transition from Stoner band model to spin-wave model. It can be seen from inset of Fig. 2 that the magnetic property in the range from 140 to 285 K is different from that in temperature region from 80 to 115 K.

The isothermal magnetization *M* (*H*) with magnetic fields up to 1.0 T at 300 K was measured and is shown in inset of Fig. 1. The magnetic moment is not saturated in a 1.0 T magnetic field. The saturation magnetic moment, 1.29 μ_B/fu (300 K), was obtained by plotting *M* (300 K) versus 1/*H* and extrapolating to 1/*H* = 0. The spontaneous magnetic moment *M* (300 K) = 0.87 μ_B/fu can be obtained by linear extrapolation of the high-field slope to zero field on *M–H* curve.

The $\rho(T)$ curves registered upon warming in zero and 0.5 T magnetic fields are shown in Fig. 4. The resistivity in zero and 0.5 T magnetic fields reduces with temperature decreasing from 282 to 78 K, indicating that the sample exhibits metallic behavior in this temperature range. The ratios of $\rho_{(0.0\ T,\ 282\ K)}/\rho_{(0.0\ T,\ 78\ K)}$ and $\rho_{(0.5\ T,\ 282\ K)}/\rho_{(0.5\ T,\ 78\ K)}$ are only as large as

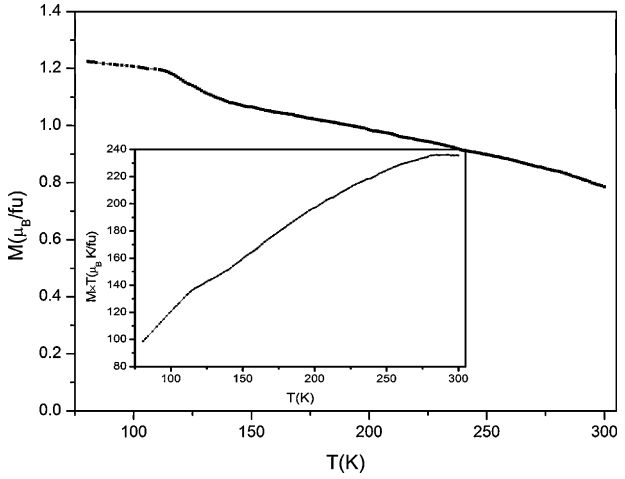

Fig. 2. *M* versus *T* for $Sr_2FeMo(O,N)_6$ measured with applied field 0.5 T; inset: $M \times T - T$ curve.

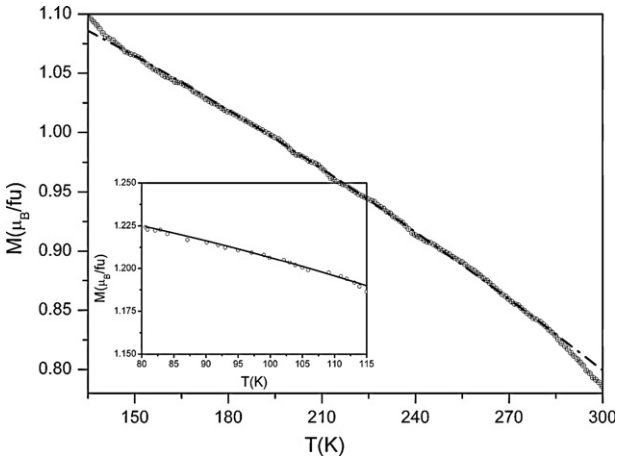

Fig. 3. Magnetization as a function of $T^{3/2}$ in the temperature region from 140 to 285 K; inset: magnetization follows T^2 in the temperature range of 80–115 K.

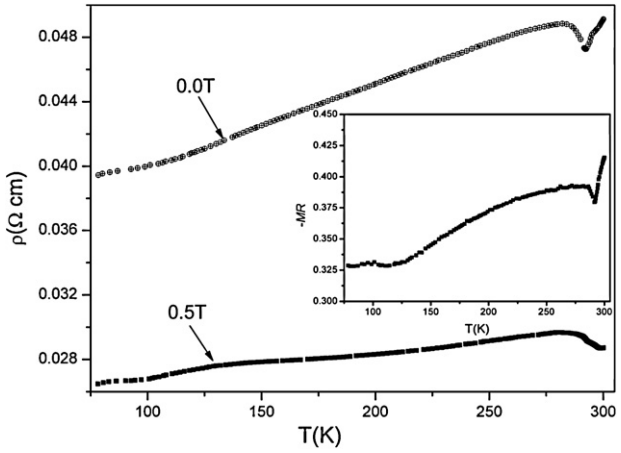

Fig. 4. Temperature dependence of resistivities registered upon warming in zero, 0.5 T magnetic fields; inset: temperature dependence of the magnetoresistance under a 0.5 T magnetic field.

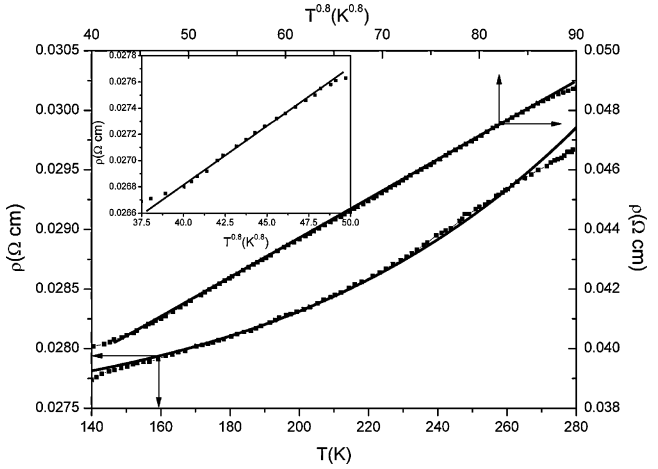

Fig. 5. Fitting of resistivities registered upon warming in a zero magnetic field to $\rho = \rho_0 + \alpha T^{0.8}$ (referred top horizontal axis and right vertical axis) and in a 0.5 T magnetic field to $\rho = \rho_0 + \beta T^2 + \gamma T^{4.5}$ (referred bottom horizontal and left vertical axis) in temperature range from 145 to 267 K; inset: fitting of resistivity data under a 0.5 T magnetic field to $\rho = \rho_0 + \alpha T^{0.8}$ in temperature region of 97–130 K.

1.24 and 1.12, respectively. Anomalies are displayed on the $\rho(T)$ dependence from 282 to 300 K in zero and 0.5 magnetic fields, respectively, which coincides with the anomaly on $M \times T$–T curve in temperature range from 282 to 300 K (see inset of Fig. 2, temperature dependence of $M \times T$ is almost unchanged). This indicates that the electrical behavior correlates with magnetic properties. One can see from Fig. 4 that the sample shows a significant magnetoresistance (MR) in a 0.5 T magnetic field. We define $MR = [\rho(H) - \rho(0)]/\rho(0)$, where $\rho(H)$ and $\rho(0)$ are the resistivity in a magnetic field and without a magnetic field, respectively. The temperature dependence of the $-MR$ in a 0.5 T magnetic field is shown in inset of Fig. 4. It can be seen from inset of Fig. 4 that the $-MR$ shows a decreasing tendency with lowering temperature. It is known that the $-MR$ decreases monotonously with increasing temperature due to the decrease of the polarization. This implies that there exists another component in which spin polarization increases with increasing temperature. We expect that the impurity of iron oxide plays an important role for explaining experimental result as spin polarization in antiferromagnetic iron oxide increases with increasing temperature below its Neel temperature.

Since there are anomalies on the $\rho-T$ curves at low and high temperature ranges, respectively, we only analyze the electrical transport behavior in middle temperature range. The resistivity under zero and 0.5 T magnetic fields in the middle temperature range was fitted following equations:

$$\rho = \rho_0 + \alpha T^n \quad (1)$$

$$\rho = \rho_0 + \beta T^2 + \gamma T^{4.5} \quad (2)$$

where ρ_0 is the residual resistivity at $T = 0$ K, α is the constant. β is electron–electron scattering coefficient and γ is electron–magnon scattering coefficient [15]. Fig. 5 shows the fitting of resistivity under a zero magnetic field to Eq. (1) (referred top horizontal axis and right vertical axis) in the temperature range from 108 to 274 K and n obtained from fitting is 0.8, close to 1. This implies that the electrical transport behavior is mostly controlled by electron–phonon scattering [16]. Fig. 5 also shows the fitting of resistivity under a 0.5 T field to Eq. (2) (referred bottom horizontal and left vertical axis) in the temperature range from 145 to 267 K. This indicates that the electrical transport behavior correlates with magnon. The coefficients of β and γ can be obtained from the fitting result and are 1.303×10^{-8} Ω cm/K^2 and 1.295×10^{-14} Ω cm/K$^{4.5}$, respectively. The last term, γ, is large enough that the contribution of the two-magnon scattering is significant [17], indicating that iron oxide probably joins in spin polarization. Inset of Fig. 5 shows the fitting of resistivity in a 0.5 T field to Eq. (1) in the temperature range from 97 to 130 K and the fitting value of n, 0.8, is same as that in a zero field, indicating that electrical transport behavior is dominantly governed by electron–phonon scattering in low temperature range. From analysis of magnetic properties and electrical transport behavior in a magnetic field and without a magnetic field we can derive that a collective excitation of the electron spin is induced by incorporation of a magnetic field and temperature in the middle temperature range.

4. Conclusions

We have investigated the crystal structure, magnetic properties, magnetoresistance and electrical transport behavior of nitrogen-doped in Sr_2FeMoO_6. The X-ray diffraction pattern shows that most cations of Fe and Mo orderly occupy on B′- and B″-sites, respectively. Thermal magnetization analysis shows that the spontaneous magnetization follows Stoner band model in the region of 80–115 K and spin wave theory in the temperature range from 140 to 285 K, respectively. Thermal magnetization shows that magnetic structure appears a change at 282 K. The magnetoresistance reduces with decreasing temperature. The electrical transport behavior demonstrates that the resistivity is controlled by electron–phonon scattering

under a zero magnetic field in the temperature range from 108 to 274 K and by electron–electron and electron–magnon scattering under a 0.5 T magnetic field in the temperature range from 145 to 267 K, respectively. The electrical transport behavior demonstrates that the resistivity is almost governed by electron–phonon scattering under a 0.5 T magnetic field in the temperature region from 97 to 130 K, however.

Acknowledgment

This work was supported by the Natural Science Foundation of Hebei Province (No. B2004000095).

References

[1] K.I. Kobayashi, T. Kimura, H. Sawada, K. Terakura, Y. Tokura, Room-temperature magnetoresistance in an oxide material with an ordered double-perovskite structure, Nature 395 (1998) 677–680.

[2] T.H. Kim, M. Uehara, S.W. Cheong, S. Lee, Large room-temperature intergrain magnetoresistance in double perovskite $SrFe_{1-x}(Mo\ or\ Re)_xO_3$, Appl. Phys. Lett. 74 (1999) 1737–1739.

[3] D.D. Sharma, P. Mahadevan, D.T. Saha, S. Ray, A. Kumar, Electronic structure of Sr_2FeMoO_6, Phys. Rev. Lett. 85 (2000) 2549–2552.

[4] O. Chmaissem, R. Kruk, B. Dabrowski, D.E. Brown, X. Xiong, S. Kolesnik, J.D. Jorgensen, C.W. Kimbal, Structural phase transition and the electronic and magnetic properties of Sr_2FeMoO_6, Phys. Rev. B 62 (2000) 14197–14206.

[5] Y. Tomioka, T. Okuda, Y. Okimoto, R. Kumai, K.I. Kobayashi, Y. Tokura, Magnetic and electronic properties of a single crystal of ordered double perovskite Sr_2FeMoO_6, Phys. Rev. B 61 (2000) 422–427.

[6] L. Balcells, J. Navarro, M. Bibes, A. Roig, B. Martinez, J. Fontcuberta, Cationic ordering control of magnetization in Sr_2FeMoO_6 double perovskite, Appl. Phys. Lett. 78 (2001) 781–783.

[7] A.H. Habib, C.V. Tomy, A.K. Nigam, D. Bahadur, Structural, transport and magnetic properties of $Sr_{2-x}Nd_xFeMoO_6$ ($0 \leq x \leq 1$), Physica B 362 (2005) 108–117.

[8] D. Serrate, J.M.D. Teresa, J. Blasco, M.R. Ibarra, L. Morellon, Large low-field magnetoresistance and T_C in polycrystalline $(Ba_{0.8}Sr_{0.2})_{2-x}La_xFeFeMoO_6$ double perovskites, Appl. Phys. Lett. 80 (2002) 4573–4575.

[9] X.M. Feng, G.H. Rao, G.Y. Liu, W.F. Liu, Z.W. Ouyang, J.K. Liang, Enhancement of Curie temperature and room-temperature magnetoresistance in double perovskite $(Sr_{1.6}Ba_{0.4})FeMoO_6$, Solid State Commun. 129 (2004) 753–755.

[10] J. Navarro, C. Frontera, L. Balcells, B. Martinez, J. Fontcuberta, Raising the Curie temperature in Sr_2FeMoO_6 double perovskites by electron doping, Phys. Rev. B 64 (2001), 092411(1–4).

[11] M. Retuerto, J.A. Alonso, M.J. Martinez-Lope, J.L. Martinez, M. Garcia-Hernandez, Record saturation magnetization, Curie temperature, and magnetoresistance in Sr_2FeMoO_6 double perovskite synthesized by wet-chemistry techniques, Appl. Phys. Lett. 85 (2004) 266–268.

[12] T.S. Chan, R.S. Liu, G.Y. Guo, S.F. Hu, J.G. Lin, J.M. Chen, C.-R. Chang, Effects of B′-site transition metal on the properties of double perovskites Sr_2FeMO_6 (M = Mo, W): B′ 4d–5d system, Solid State Commun. 133 (2005) 265–270.

[13] K. Wang, Y. Sui, Influence of the modulating interfacial state on Sr_2FeMO_6 powder magnetoresistance properties, Solid State Commun. 129 (2004) 135–138.

[14] I.D. Brown, D. Altermatt, Bond-valence parameters obtained from a systematic analysis of the inorganic crystal structure database, Acta Cryst. 41 (1985) 244–247.

[15] G.J. Synder, R. Hiskes, S. DiCarolis, M.R. Beasley, T.H. Geballe, Intrinsic electrical transport and magnetic properties of $La_{0.67}Ca_{0.33}MnO_3$ and $La_{0.67}Sr_{0.33}MnO_3$ MOCVD thin films and bulk material, Phys. Rev. B 53 (1996) 14434–14444.

[16] Z. Boekelheide, D.W. Cooke, E. Helgren, F. Hellman, Resonant impurity scattering and electron–phonon scattering in the electrical resistivity of Cr thin films, Phys. Rev. B 80 (2009), 134426(1–12).

[17] Sh. Dong, H. Yu, K.-F. Wang, X.Y. Yao, J.-M. Liu, Phase separation and magnetoresistance on random-field magnetic polaron system, Comput. Mater. Sci. 33 (2005) 168–174.